Measurements of surface scattering mean-free paths in coarse-grain steel samples with a multielement array

Clément Du-Burck, Arnaud Derode

MEASUREMENTS OF SURFACE SCATTERING MEAN-FREE PATHS IN COARSE-GRAIN STEEL SAMPLES WITH A MULTIELEMENT ARRAY

Clément du Burck[1] **Arnaud Derode**[1]
[1] ESPCI Paris, PSL University, CNRS, Université de Paris,
Institut Langevin, 1 rue Jussieu, 75005 Paris, France
clement.du-burck@espci.fr arnaud.derode@espci.fr

ABSTRACT

A study of frequency-dependent scattering mean-free paths of two ballistic waves in polycrystalline media is presented. Experimental data sets are obtained by recording impulse-response-type time signals using a multielement array at the surface of polycrystalline samples. Spatial averaging allows for the estimation of the coherent field in which two ballistic waves are observed. A frequency-domain method is introduced to extract the experimental scattering mean-free path of each ballistic wave between 3.5 and $7.5\,\mathrm{MHz}$. Theoretical models described in the literature are applied to also obtain theoretical scattering mean-free paths. Experimental and theoretical results are compared. The use of coherent field to extract microstructural information for non-destructive evaluation purposes is discussed.

1. INTRODUCTION

When propagating in a polycrystalline medium such as a metallic alloy, an ultrasonic wave is subject to single, and possibly multiple scattering at crystallite (or "grain") boundaries. The impedance mismatches are due to random crystalline orientations of the grains, hence to local variations of elastic constants. Scattering leads to the attenuation and diffusion of the incident wave, which can make flaw detection difficult through ultrasonic non-destructive evaluation (NDE): the ballistic wave reflected by a defect may have a lower amplitude than the back-scattered wavefield, often referred to as grain or structural noise. It should be noted that the designation "noise" is somewhat misleading, as it does not convey the fact that grain noise carries information about the microstructure of the polycrystalline medium. The aim of studies on polycrystals is thus to extract microstructural information from ultrasonic NDE measurements through the inversion of a reliable theoretical model. To this end, it is important to well understand the attenuation mechanisms in polycrystals.

Multiple theoretical models predicting attenuation coefficients in polycrystals exist, the main references being the models by Stanke and Kino [1] and by Weaver [2]. These two are known to provide results spanning multiple frequency regimes. Still, as well as nearly all other theoretical models, they focus on bulk longitudinal and transverse waves' attenuation. This is reflected by the fact that most experimental studies conducted on the attenuation in polycrystals mainly focus on grain noise, in hope of extracting information about the microstructure from isolated NDE experiments by studying the statistics of grain noise, i.e., of the "incoherent field" (or *coda*). Unlike grain noise, the "coherent field" resists to ensemble averages. Ryzy *et al.*'s recent publication [3] studies the possibility of deriving microstructural information not from grain noise, but from the coherent field – more specifically, from coherent surface waves.

In this paper, we propose to apply Weaver's model and then to follow Ryzy *et al.*'s procedure to compute theoretical scattering mean-free paths of two coherent ballistic waves in Inconel® 600 polycrystalline alloys: a surface-skimming longitudinal wave and a surface Rayleigh wave. As these two waves are experimentally observed in the estimated coherent field on two samples with different grain size distributions, comparisons between experimental and theoretical results are made possible. In Sec. 2, the experimental estimation of the coherent field using a multielement array is described. The advantage of the experimental setup presented here is its simplicity and wieldiness compared to the opto-acoustic setup used by Ryzy *et al.*; on the other hand, the frequency bandwidth is much smaller than that of measurements made using an opto-acoustic setup. From the estimated coherent field, a frequency-domain – or "monochromatic" –, procedure is described in Sec. 3 to measure the experimental scattering mean-free path of each of the two observed ballistic waves. Then, theoretical scattering mean-free paths are derived using models presented in Sec. 4 and are compared with experimental results.

2. EXPERIMENTAL SETUP

2.1 Inspected Polycrystalline Media

For this study, two blocks of polycrystalline Inconel® 600 (alloy made for the most part of nickel, chromium and iron) of section $90 \times 90\,\mathrm{mm}^2$ were used. These blocks were manufactured by EDF R&D as part of a collaboration, and their respective microstuctures have previously been studied [4]. In particular, the mean grain diameter d of each block is known: one block's microstructure consists of small grains ($d = 89.2\,\mu\mathrm{m}$) and the other one's of large grains ($d = 748\,\mu\mathrm{m}$); hence, these blocks will be referred to as "small-grain block" and "coarse-grain block"

ρ (mg/mm^3)	c_{11} (GPa)	c_{12} (GPa)	c_{44} (GPa)
8.26	234.6	145.4	126.2

Table 1. Density and elastic constants of a single cubic crystal of Inconel® 600 [5].

respectively in the following. Furthermore, elastic properties of a single cubic crystal of Inconel® 600 are known [5] and given in Tab. 1.

2.2 Measurement of Ballistic Waves

Experimental data is obtained using an array of 128 transducers with central frequency 5.5 MHz. A single acquisition on a polycrystalline block consists in measuring an inter-element impulse response matrix $\mathbf{h}(t)$ with the multielement array. This matrix is obtained using a process called "full matrix capture" (FMC): time signals are recorded by every element of the array when they are individually and sequentially excited by the same impulse signal. Thus, the matrix $\mathbf{h}(t)$ has dimensions $128 \times 128 \times N_t$: the first dimension represents the source transducer, the second the receiving transducer and the third the time samples, N_t being the number of recorded time samples.

To estimate ballistic waves, part of the so-called "coherent field", it is necessary to perform an average. Rigorously, equivalent realisations of disorder should be averaged, but assuming ergodicity, this ensemble average can be replaced by a spatial average. As illustrated in Fig. 1, a set of A matrices $\mathbf{h}^{(a)}(t)$ $(1 \leq a \leq A)$ is recorded on each block by scanning its surface along its length: between two consecutive acquisitions, the array's position is shifted so that it is facing a different – and supposedly independent –, arrangement of grains. A total of $A = 72$ and of $A = 113$ matrices $\mathbf{h}^{(a)}(t)$ are recorded on the small-grain and coarse-grain blocks respectively.

The first processing performed on these two data sets is filtering: every time signal is filtered using a second order band-pass zero phase Butterworth filter with cutoff frequencies 3.5 and 7.5 MHz. All analysis described in this paper will therefore be restricted to this frequency range. Assuming statistical homogeneity and isotropy along the scanned face of each block, the average performed to estimate the coherent field is twofold: first, the A matrices $\mathbf{h}^{(a)}(t)$ are averaged; and second, time signals corresponding to the same source-receiver distance x are averaged. This provides averaged signals, noted $u(x,t)$ and represented as B-scans (images whose lines are time signals) in Fig. 2. In addition to estimating the coherent field on each block, we can estimate the statistical fluctuations ("noise") $n^{(a)}(x,t)$ of each of the A acquisitions – which will be essential to compute error bars later in this document –, by subtracting the averaged signals $u(x,t)$ to the a-th measure $h^{(a)}(x,t)$:

$$n^{(a)}(x,t) = h^{(a)}(x,t) - u(x,t). \tag{1}$$

On each of the two B-scans in Fig. 2, two ballistic waves are clearly visible. On the coarse-grain block, they appear to decay much faster than on the small-grain one, which reflects the fact that a coarse-grain microstructure scatters much more strongly than a small-grain one. In the following, the study will be focused on the two ballistic waves.

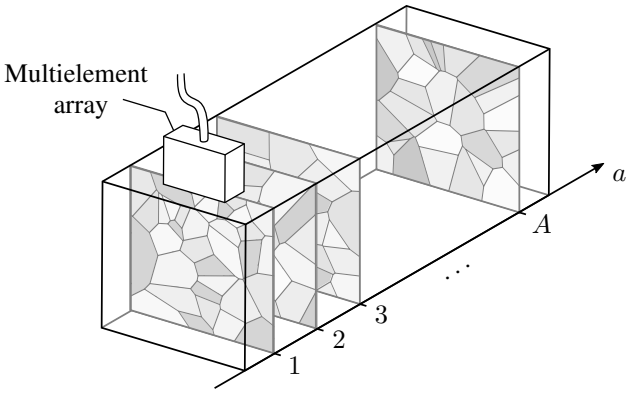

Figure 1. Illustration of the measurement of A inter-element impulse response matrices $\mathbf{h}^{(a)}(t)$ on a polycrystalline block.

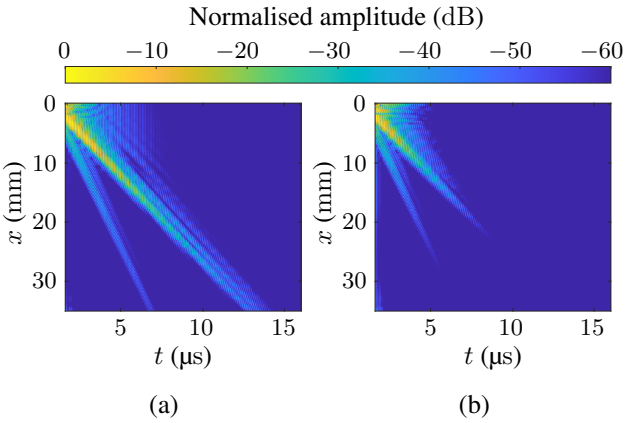

Figure 2. Averaged signals $u(x,t)$ measured (a) on the small-grain block and (b) on the coarse-grain block.

3. DATA ANALYSIS

3.1 Extraction of Scattering Mean-Free Paths

Experimentally, scattering mean-free path ℓ_s of a given wave (or equivalently, the attenuation coefficient $\alpha = 1/2\ell_s$) is linked to the decay of said wave, as scattering is known to cause an exponential attenuation $\exp(-r/2\ell_s)$ with distance r of the amplitude of a wave propagating in any direction. In this section, we propose a method to measure the experimental scattering mean-free path of each observed ballistic wave, along with an estimation of experimental uncertainty. As scattering is a frequency-dependent phenomenon, the approach presented here is monochromatic and will provide frequency-dependent mean-free paths $\ell_s(f)$. Moreover, as it will be emphasised in the following, care has to be taken because the attenuation of a

wave is not due solely to scattering, but also to the geometrical spreading of the wave. Taking these points into account, the scattering mean-free paths are estimated through the following steps.

3.1.1 Windowing of Ballistic Waves

The first step is to isolate each ballistic wave by windowing it. The window is chosen so that it "follows" the wave of interest, which requires a gross estimation of the waves' group velocities. This estimation simply consists in calculating the slope of the two ridgelines appearing on the averaged B-scans in Fig. 2. On both blocks, we find group velocities of about $5.75\,\mathrm{mm/\mu s}$ for the fast ballistic wave and $2.85\,\mathrm{mm/\mu s}$ for the slow one. From Fig. 2, it appears that on the coarse-grain block, ballistic waves decay very quickly; so quickly, in fact, that they are drowned out by the grain noise remaining after averaging for rather short distances x. Consequently, spatial windowing on the coarse-grain block will be more restrictive than on the small-grain block. Moreover, as it appears that the fast ballistic wave is less temporally spread out than the slow wave, the corresponding temporal window will be shorter. The windowed signals $\hat{u}(x,t)$ used in this paper are represented in Fig. 3. Noise $n^{(a)}(x,t)$ calculated from (1) may be windowed exactly as the averaged signals $u(x,t)$, providing a set of A windowed noise signals $\hat{n}^{(a)}(x,t)$.

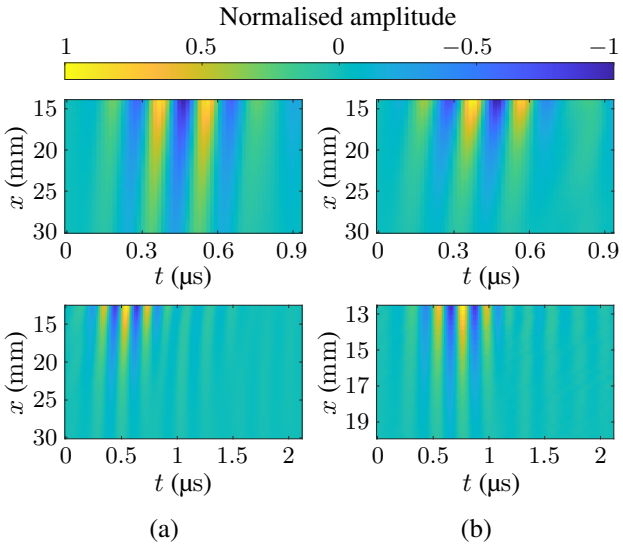

Figure 3. Windowed signals $\hat{u}(x,t)$ of the fast (top) and slow (bottom) ballistic waves measured (a) on the small-grain block and (b) on the coarse-grain block.

3.1.2 Calculation of Ballistic Waves' Attenuation

As previously mentioned, the approach proposed here is monochromatic. This implies the passage to the frequency domain by calculating the spectrum $U(x,f) = \mathrm{FT}\{\hat{u}(x,t)\}$ of each windowed ballistic wave, where $\mathrm{FT}\{\cdot\}$ designates the temporal discrete Fourier transform. At any frequency f, the wave's amplitude $|U(x,f)|$ is modelled as:

$$|U(x,f)| \propto g(x) \exp\left[-\frac{x}{2\ell_s(f)}\right], \tag{2}$$

where the term $g(x)$ represents the geometrical spreading of the studied wave. For instance, for a wave of spherical symmetry (bulk wave generated by a point source), $g(x) = 1/x$, while for a wave of cylindrical symmetry (surface wave generated by a point source), $g(x) = 1/\sqrt{x}$. From the model (2), scattering mean-free path $\ell_s(f)$ may be obtained through linear regressions at all frequencies f of the quantity $y(x,f)$ defined as:

$$y(x,f) = \log\left[\frac{|U(x,f)|}{g(x)}\right]. \tag{3}$$

Therefore, a choice has to be made for the geometrical spreading function $g(x)$ of each ballistic wave: from the relative group velocities previously estimated on both blocks, the fast ballistic wave is assumed to be a surface-skimming longitudinal wave (SSLW, also called subsurface longitudinal wave or longitudinal critically refracted wave) and the slow one a Rayleigh-type surface wave (RW). Under the hypothesis that the considered source-receiver distances x are large enough to neglect diffraction effects due to the finite size of transducers (that is, transducers are supposed to be point sources), the former has a geometrical spreading corresponding to a point-source-generated bulk longitudinal wave, hence $g(x) = 1/x$; and the latter has a cylindrical symmetry, hence $g(x) = 1/\sqrt{x}$. The variable $y(x,f)$ thus computed from (3) for each windowed ballistic wave is represented against distance x in Fig. 4 for multiple frequencies f ranging from 3.5 to 7.5 MHz.

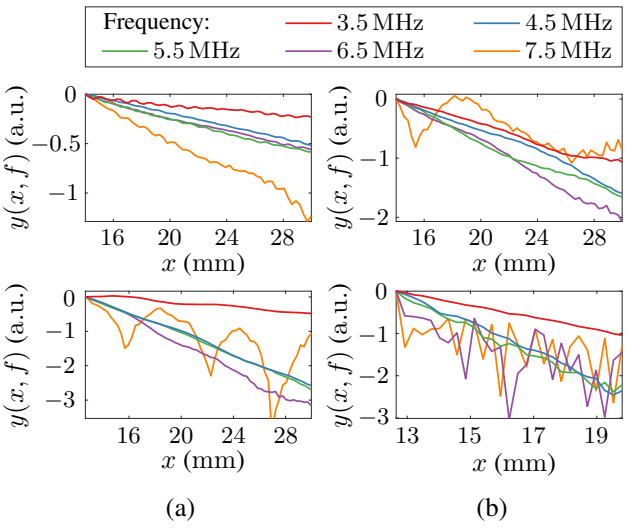

Figure 4. Natural logarithm of the amplitude $|U(x,f)|$ at multiple frequencies compensated by the geometrical spreading $g(x)$ for the fast (top) and slow (bottom) ballistic waves measured (a) on the small-grain block and (b) on the coarse-grain block. Amplitudes are normalised so that $|U(x,f)|/g(x) = 1$ at the minimum distance x.

As a first observation, it appears that the slope of $y(x,f)$ is lower in magnitude, i.e., attenuation due to scattering is less important, at low frequencies. This is a known result: the attenuation coefficient increases with frequency up until the high-frequency regime (often called "geometrical regime"), where it becomes frequency-independent. From Fig. 4, it seems that the grain noise remaining after averaging prevents the use of the method described here for the calculation of $\ell_s(f)$ at high frequencies. In other words, there is not enough experimental data to average out the grain noise. This is especially apparent on the coarse-grain block and for the slow wave, as both display non-linear curves $y(x,f)$ at high frequencies. This observation leads us to consider the signal-to-noise ratio (SNR) as a means to decide if the curve $y(x,f)$ at a given frequency f should be fitted or not. The SNR, as a function of distance x and frequency f, is calculated as:

$$\mathrm{SNR}(x,f) = \frac{|U(x,f)|}{\sigma_U(x,f)}, \tag{4}$$

where $\sigma_U(x,f)$ represents the uncertainty of the amplitude $|U(x,f)|$. In order to estimate $\sigma_U(x,f)$, the spectrum $N^{(a)}(x,f) = \mathrm{FT}\{\hat{n}^{(a)}(x,t)\}$ of the windowed noise is computed and its variance $\sigma_N^2(x,f)$ is estimated:

$$\sigma_N^2(x,f) = \frac{1}{A}\sum_{a=1}^{A} |N^{(a)}(x,f)|^2. \tag{5}$$

The uncertainty $\sigma_U(x,f)$ is finally given by:

$$\sigma_U(x,f) = \sqrt{\frac{\sigma_N^2(x,f)}{A}}. \tag{6}$$

To simplify matters, the SNR calculated from (4) is averaged over distances x, so that it becomes a function of the sole frequency variable f: the SNRs considered in the following will be noted $\langle \mathrm{SNR} \rangle_x(f)$. In Fig. 5, SNRs for each windowed ballistic wave considered in this paper are represented against frequency.

As it had been observed from Fig. 4, the SNRs of the windowed slow wave on each block become particularly

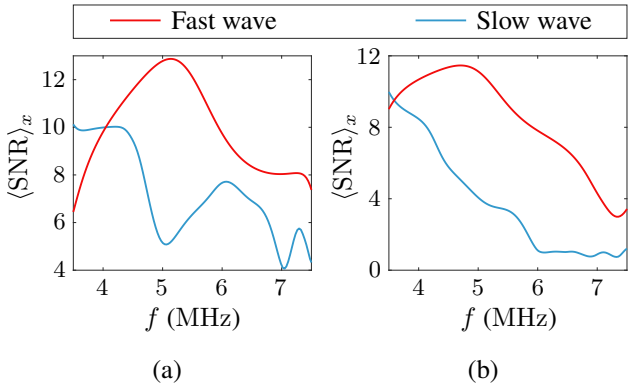

Figure 5. Signal-to-noise ratios of the two windowed ballistic waves measured (a) on the small-grain block and (b) on the coarse-grain block. SNRs are averaged over distances x to be represented as a function of frequency f.

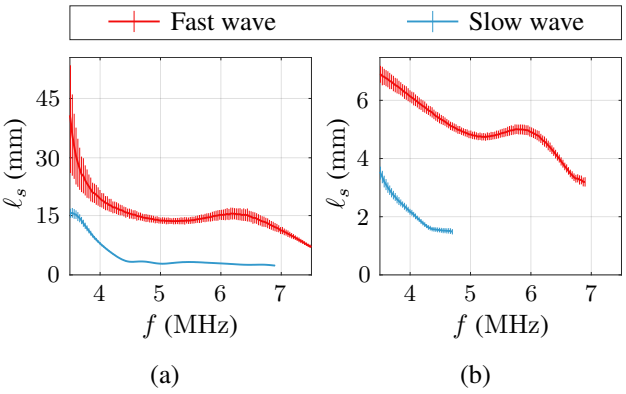

Figure 6. Scattering mean-free paths with error bars of the two windowed ballistic waves measured (a) on the small-grain block and (b) on the coarse-grain block. Results are given for frequencies f verifying the criterion (7).

small at high frequencies (it actually falls to unity on the coarse-grain block over 6 MHz). To avoid noise-related difficulties, only frequencies verifying the following criterion will be considered in this paper:

$$\langle \mathrm{SNR} \rangle_x(f) \geq 5. \tag{7}$$

Taking this criterion into account, the measured scattering mean-free paths $\ell_s(f)$ are given in Fig. 6. The error bars displayed in this figure are obtained through a Monte-Carlo procedure, performed using the uncertainty $\sigma_y(x,f)$. From the expression of $y(x,f)$ in (3), one obtains its uncertainty $\sigma_y(x,f)$ from $\sigma_U(x,f)$ by:

$$\sigma_y(x,f) = \frac{\sigma_U(x,f)}{|U(x,f)|}. \tag{8}$$

3.2 Validity of Ballistic Waves' Modelling

In the previous section, scattering mean-free paths $\ell_s(f)$ were calculated for the two ballistic waves appearing on each polycrystalline block by performing linear regressions of the quantity $y(x,f) = \log[A(x,f)/g(x)]$ at all frequencies f. This implied modelling the two ballistic waves' geometrical spreading $g(x)$: the fast and slow waves, supposedly a SSLW and a RW, decay as $g(x) = 1/x$ and $g(x) = 1/\sqrt{x}$ respectively. In this section, we propose to test the validity of these models with a simple statistical test. The experimental data $y(x,f)$ at a given frequency f is compared to the linear fit $y^{\mathrm{fit}}(x,f)$, taking into account the uncertainty $\sigma_y(x,f)$. To this end, the proportion $P(f)$ of the line $y^{\mathrm{fit}}(x,f)$ intercepting the experimental data to within two standard deviations $(y(x,f) \pm 2\sigma_y(x,f))$ is measured: assuming normally distributed noise, the chosen model for $g(x)$ is accepted if the proportion is greater than 95 %; otherwise, it is rejected. As the proportions $P(f)$ measured for each windowed ballistic wave equal 100 % at all frequencies verifying the criterion (7), the chosen models for $g(x)$ seem accurate. Note however that the test performed here does not prove the validity of these models but simply points towards it.

4. COMPARISON TO THEORETICAL MODELS

Multiple theoretical models exist to describe bulk waves' attenuation in polycrystals. Stanke and Kino's [1] and Weaver's [2] models are usually considered as references nowadays for crystallites of cubic symmetry. Unlike historically previous models, these two provide results spanning multiple frequency regimes.

In this section, theoretical scattering mean-free paths are computed using Weaver's model and are compared to the experimentally obtained curves of $\ell_s(f)$. To this end, we first apply Weaver's model [2] in its simplest form to obtain bulk longitudinal and transverse waves' attenuation, implying a few hypotheses that will be mentioned; then the Rayleigh wave's attenuation coefficient is calculated through a procedure proposed by Ryzy *et al.* [3].

4.1 Bulk Waves' Attenuation

In his theoretical model, Weaver studied bulk ultrasonic waves' diffusivity in polycrystals and obtained closed-form expressions for the attenuation coefficients $\alpha_L(f)$ and $\alpha_T(f)$ of longitudinal and transverse waves respectively. Weaver's model, as Stanke and Kino's, makes use of a function $W(\mathbf{r})$ called "two-point correlation function" (TPCF), representative of the microstructure's statistics: $W(\mathbf{r})$ is defined as the probability that two points separated by a vector $\mathbf{r}$ within the microstructure are located in the same grain. By definition, $W(\mathbf{0}) = 1$ and $W(\mathbf{r}) \to 0$ when $|\mathbf{r}| \to \infty$, but the exact form of a given microstructure's TPCF is not trivial. The TPCF is an important part of Weaver's model as its spatial Fourier transform appears in the expressions of attenuation coefficients. As we assumed statistical isotropy in the studied polycrystalline samples, the TPCF is actually a function of the distance $r = |\mathbf{r}|$. To further simplify matters, we will make the recurrent, though debatable, assumption that the TPCF follows an exponential law:

$$W(r) = \mathrm{e}^{-r/\ell_c}, \tag{9}$$

where ℓ_c, called "correlation length", is a characteristic length describing the microstructure. The exponential form for the TPCF is often discussed in the literature and the choice of the length ℓ_c is not necessarily unique. In particular, it has been observed that while the exponential form may be suited to some cases, a single characteristic length ℓ_c is rarely enough to fully describe the statistics of the microstructure. For example, taking into account the grain size distribution's mean and deviation has shown different results than using the mean of the distribution alone [6]. However, as the experimental TPCFs of the studied blocks have yet to be measured, we will settle for the exponential form TPCF (9) and will assume the correlation length ℓ_c to be equal to the known mean grain diameter d. Under the hypothesis of an exponential TPCF, Weaver fully calculated attenuation coefficients $\alpha_L(f)$ and $\alpha_T(f)$ (Eqs. (7.11) to (7.14) of reference [2]). These expressions depend on the correlation length ℓ_c, on the cubic crystal anisotropy factor $\nu = c_{11} - c_{12} - 2c_{44}$ (calculated from elastic constants in Tab. 1), but also on "homogenised wave velocities" c_L and c_T; that is, wave velocities considering the polycrystal as a homogeneous and isotropic medium with elastic properties obtained from single crystal elastic constants and density. As in Stanke and Kino's model, Weaver expressed c_L and c_T through a Voigt homogenisation technique, providing:

$$c_L = \sqrt{\frac{3c_{11} + 2c_{12} + 4c_{44}}{5\rho}}, \tag{10}$$

$$c_T = \sqrt{\frac{c_{11} - c_{12} + 3c_{44}}{5\rho}}. \tag{11}$$

Then again, the choice of a Voigt averaging is questionable, as it has been shown that this homogenisation overestimates wave velocities [7]. Other averaging methods exist, some of them being discussed in reference [8], but we will consider the Voigt homogenisation in this section, as in most of the literature. Homogenised wave velocities considered here are thus given by (10) and (11).

4.2 Rayleigh Wave's Attenuation

From the last section, attenuation coefficients $\alpha_L(f)$ and $\alpha_T(f)$ of bulk longitudinal and transverse waves are known. Weaver's model, however, does not describe attenuation of surface waves. In order to compute the attenuation coefficient $\alpha_R(f)$ of Rayleigh waves, we use a procedure introduced by Ryzy *et al.* in reference [3], allowing calculation of $\alpha_R(f)$ from the knowledge of $\alpha_L(f)$ and $\alpha_T(f)$. The objective of this procedure is to calculate the RW's complex wavenumber $\tilde{k}_R(f) = k_R(f) + \mathrm{i}\alpha_R(f)$, where $k_R(f) = 2\pi f/c_R(f)$ is the RW's real wavenumber, $c_R(f)$ being the RW's velocity. To this end, we first introduce the Rayleigh equation written in terms of real wavenumbers $k_i(f)$ ($i = L, T, R$) [9]:

$$\gamma^6 - 8\gamma^4 + 8(3 - 2\kappa^{-2})\gamma^2 - 16(1 - \kappa^{-2}) = 0, \tag{12}$$

where $\gamma = k_T/k_R$ and $\kappa = k_T/k_L$. Assuming small attenuation coefficients compared to real wavenumbers, i.e., $\alpha_i(f) \ll k_i(f)$, Ryzy *et al.* proposed replacing real wavenumbers $k_i(f)$ in the Rayleigh equation (12) by their complex counterparts $\tilde{k}_i(f)$, which gives the "complex Rayleigh equation":

$$\tilde{\gamma}^6 - 8\tilde{\gamma}^4 + 8(3 - 2\tilde{\kappa}^{-2})\tilde{\gamma}^2 - 16(1 - \tilde{\kappa}^{-2}) = 0, \tag{13}$$

where $\tilde{\gamma} = \tilde{k}_T/\tilde{k}_R$ and $\tilde{\kappa} = \tilde{k}_T/\tilde{k}_L$. This equation may be resolved numerically at all frequencies, thus providing the attenuation coefficient $\alpha_R(f)$. As well as for the real Rayleigh equation (12), the physically relevant solution of the complex Rayleigh equation (13) has to be chosen from the six mathematical roots obtained at a given frequency. This choice may be done by looking for the root whose real part is the closest to an approximation of the RW's real wavenumber $\hat{k}_R(f) = 2\pi f/\hat{c}_R$, where $\hat{c}_R$ is an approximation of the RW's velocity; for example, Royer and Clorennec proposed an approximation $\hat{c}_R$ [10], which, coupled with Voigt averaging, reads:

$$\hat{c}_R = c_T\sqrt{\frac{116c_{11} + 244c_{12} - 12c_{44}}{137c_{11} + 258c_{12} + 16c_{44}}}, \tag{14}$$

where c_T is given by (11).

To ensure the validity of the method described in this section, one has to verify the hypothesis $\alpha_i(f) \ll k_i(f)$ for all waves (i.e., for $i = L, T, R$). Hence, attenuation coefficients $\alpha_i(f)$ are computed using Weaver's model and Ryzy *et al.*'s procedure as described previously for the two polycrystalline blocks studied here, and the maximum value of $\alpha_i(f)/k_i(f)$ over the frequency range spanning from 3.5 to 7.5 MHz is calculated for each wave. These maxima are given in Tab. 2. It appears that $\alpha_T(f)$ and $\alpha_R(f)$ respectively reach up to about a fifth of $k_T(f)$ and $k_R(f)$ on the coarse-grain block, hence the hypothesis $\alpha_i(f) \ll k_i(f)$ may not hold true on this block.

Block	$\max\left(\frac{\alpha_L}{k_L}\right)$	$\max\left(\frac{\alpha_T}{k_T}\right)$	$\max\left(\frac{\alpha_R}{k_R}\right)$
SG	1.05×10^{-2}	2.11×10^{-2}	1.99×10^{-2}
CG	1.89×10^{-2}	2.11×10^{-1}	1.94×10^{-1}

Table 2. Maximum values of the ratios $\alpha_i(f)/k_i(f)$ ($i = L, T, R$) for frequencies ranging from 3.5 to 7.5 MHz on each studied polycrystalline block. SG and CG stand for small-grain and coarse-grain blocks respectively.

4.3 Comparison with Experimental Results

As theoretical attenuation coefficients $\alpha_i(f)$ are computed as described in the two previous sections, they may be compared with experimentally measured scattering mean-free paths. As the fast ballistic wave is assumed to be a surface-skimming longitudinal wave, its experimental scattering mean-free path $\ell_s(f)$ is to be compared with half the inverse of the bulk longitudinal wave's theoretical attenuation coefficient calculated from Weaver's model ($1/2\alpha_L(f)$). As for the slow ballistic wave, supposedly a Rayleigh wave, its experimental scattering mean-free path $\ell_s(f)$ shall be compared with $1/2\alpha_R(f)$, where $\alpha_R(f)$ is calculated using Ryzy *et al.*'s method. These comparisons are displayed in Fig. 7.

It appears that, despite the numerous approximations that were made – the main ones being the exponential form (9) for the TPCF, the choice of the correlation length $\ell_c = d$ and the Voigt averaging –, the theoretical curves in Fig. 7 seem to roughly follow experimental scattering mean-free paths for the two ballistic waves on the small-grain block, and for the fast ballistic wave only on the coarse-grain block. The theoretical curve $1/2\alpha_R(f)$ on the coarse-grain block appears, however, to be way off the measured scattering mean-free path $\ell_s(f)$. More precisely, the experimental RW's scattering mean-free path on the coarse-grain block is much larger than the theoretical one, which means that in this case, the theory overestimates the scattering "strength". A way to quantify this observation is to compute the mismatch ϵ_i of each couple of experimental and theoretical curves:

$$\epsilon_i(f) = \frac{|\ell_s(f) - 1/2\alpha_i(f)|}{1/2\alpha_i(f)}. \qquad (15)$$

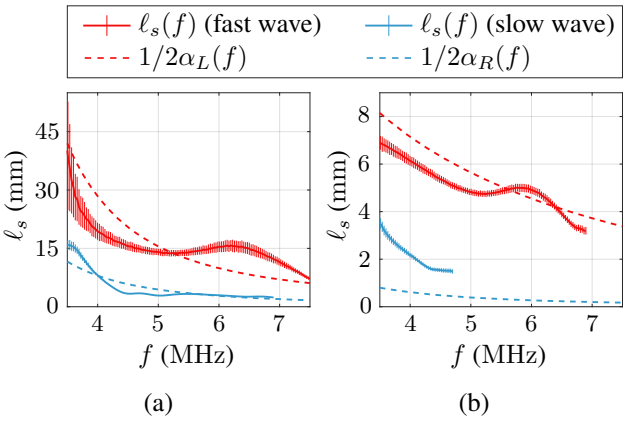

Figure 7. Comparison between the experimentally measured scattering mean-free paths $\ell_s(f)$ shown in Fig. 6 and theoretical ones calculated using Weaver's and Ryzy *et al.*'s models for the two windowed ballistic waves (a) on the small-grain block and (b) on the coarse-grain block.

On the small-grain and coarse-grain blocks respectively, ϵ_L reaches 80 % and 46 %, while ϵ_R reaches 16 % and 350 %.

The observed discrepancy between experimental and theoretical RW's scattering mean-free paths on the coarse-grain block may be due to different factors. First, as it has been observed in the last section, the hypothesis $\alpha_i(f) \ll k_i(f)$ for each wave, necessary for the calculation of $\alpha_R(f)$, is not quite verified on the coarse-grain block (Tab. 2). Moreover, the wavelength-to-mean grain diameter ratio λ/d is less than unity over 4.5 MHz for the bulk transverse wave on the coarse-grain block, which might imply that the application of Weaver's model is not really adequate at such frequencies.

Otherwise, the fact that, aside from the RW on the coarse-grain block, experimental and theoretical scattering mean-free paths seem to follow the same tendency is encouraging for the use of Weaver's and Ryzy *et al.*'s models; though the relevancy of these theoretical models in our case should not be taken as granted from the results presented here. Theoretical attenuation coefficients calculated from Weaver's model assuming an exponential TPCF highly depend, usually non-linearly, on the correlation length ℓ_c. This is shown in Fig. 8, representing the variations against correlation length ℓ_c of theoretical scattering mean-free paths at the lowest frequency $1/2\alpha_{L,R}(3.5\,\text{MHz})$ calculated using Weaver's and Ryzy *et al.*'s models. It appears that the choice of ℓ_c can have a large impact on results obtained with the small-grain block's properties: simply halving the correlation length ($\ell_c = d/2$) modifies theoretical scattering mean-free paths by a factor of about four; and setting $\ell_c = d/3$ multiplies theoretical curves in Fig. 7a by about fourteen. As for the coarse-grain block, $1/2\alpha_L$ seems to show very little dependence on the correlation length, while $1/2\alpha_R \propto 1/\ell_c$.

The previous observations partly show the limitations of the exponential form TPCF in theoretical modelling: a more precise representation would require the experimental measurement of the studied polycrystalline blocks'

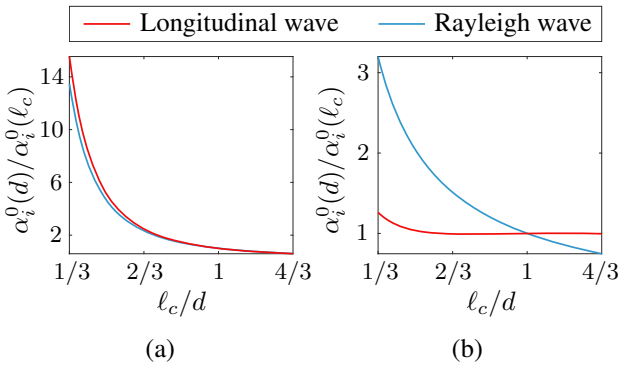

Figure 8. Variations against correlation length ℓ_c of the inverse of $\alpha_i^0 = \alpha_{L,R}(3.5\,\mathrm{MHz})$, where α_i^0 are calculated using Weaver's and Ryzy *et al.*'s models with the properties (a) of the small-grain block and (b) of the coarse-grain block. Vertical axes are normalised so that the curves equal unity when $\ell_c = d$.

TPCF. Moreover, the Voigt averaging used to calculate wave velocities c_L and c_T appearing in Weaver's model is known to provide inaccurate results. Besides, Weaver's model might not be exactly suited to the present case, as it gives attenuation coefficients $\alpha_{L,T}(f)$ that only increase with frequency ($\alpha_{L,T}(f) \propto f^n$ with $n = 4$ for $\lambda \gg d$ and $n = 2$ for $\lambda \sim d$); i.e., theoretical scattering mean-free paths calculated using Weaver's model can only decrease with frequency. This implies that Weaver's model cannot account for the "hump" that can be observed on experimental SSLWs' scattering mean-free paths $\ell_s(f)$ at around 6 MHz (Fig. 7). It shall first be confirmed, however, that this hump is not an artefact due to insufficient experimental data sets.

5. CONCLUSION

A simple experimental setup was proposed for the estimation of coherent ballistic waves in polycrystalline media using a multielement array, by scanning the surface of a sample and measuring at each position of the array an inter-element impulse response matrix $\mathbf{h}(t)$. Experimental data sets were measured on two Inconel® 600 blocks with different grain size distributions. On both blocks, two ballistic waves were observed. The fast one (group velocity of about $5.75\,\mathrm{mm/\mu s}$) is supposed to be a surface-skimming longitudinal wave and the slow one (group velocity of about $2.85\,\mathrm{mm/\mu s}$) a Rayleigh wave. From these ballistic waves, a monochromatic procedure to extract experimental, frequency-dependent, scattering mean-free paths $\ell_s(f)$ was presented, along with an estimation of experimental uncertainty. This method presumes the geometrical spreading function $g(x)$ of each studied wave to be known, therefore the assumptions made on the nature of the two ballistic waves are paramount. For this reason, a simple statistical test using the estimated uncertainty was performed to verify the validity of the choice of $g(x)$ for each ballistic wave. Besides, the presented method requires a high signal-to-noise ratio to provide reliable results and thus, large data sets are necessary in order to well-estimate coherent ballistic waves; this becomes a problem at low wavelength-to-mean grain diameter (and mean-free path-to-distance) ratios, as the signal-to-noise ratio drops with frequency and source-receiver distance.

Experimental scattering mean-free paths were compared with theoretical ones, obtained by first applying Weaver's model [2] (to obtain bulk longitudinal and transverse waves' attenuation coefficients), and then using the procedure suggested by Ryzy *et al.* [3] (to obtain the Rayleigh wave's attenuation coefficient). Weaver's model was used in its most simplified form, which assumes the two-point correlation function $W(\mathbf{r})$, describing the microstructure's statistics, to be exponentially decreasing with distance $r = |\mathbf{r}|$. Although such an approximation is often debated in the literature, a rather good quantitative agreement between theoretical and experimental scattering mean-free paths was found on the small-grain block. On the coarse-grain block, however, the experimental Rayleigh wave's scattering mean-free path appeared to be more than three times larger than the theoretical one, which might suggest the invalidity of the used theoretical model when the wavelength becomes lower than the mean-grain diameter. Nonetheless, as the importance of the correlation length ℓ_c – that is, the characteristic extinction length of the exponential function $W(r)$ –, was shown, it is clear that to reach a conclusion on the previous point, $W(r)$ should be measured experimentally on each studied sample, thus allowing the use of Weaver's model without making assumptions on the microstructure. Hence, further experimental studies are necessary to better understand and analyse differences between theoretical models and experimental results.

6. ACKNOWLEDGEMENTS

The authors wish to acknowledge the contribution from Claire Prada and Cécile Brütt for numerous scientific advice and discussions. We thank Andreas Schumm and Antoine Ferré for providing the samples, as part of a collaboration between EDF Labs at Les Renardières and Institut Langevin.

7. REFERENCES

[1] F. E. Stanke and G. S. Kino, "A unified theory for elastic wave propagation in polycrystalline materials," *J. Acoust. Soc. Am.*, vol. 75, no. 3, pp. 665–681, 1984.

[2] R. L. Weaver, "Diffusivity of ultrasound in polycrystals," *J. Mech. Phys. Solids*, vol. 38, no. 1, pp. 55–86, 1990.

[3] M. Ryzy, T. Grabec, J. A. Österreicher, M. Hettich, and I. A. Veres, "Measurement of coherent surface acoustic wave attenuation in polycrystalline aluminum," *AIP Adv.*, vol. 8, no. 12, p. 125019, 2018.

[4] S. Shahjahan, *Étude expérimentale et numérique d'un procédé de détection de défauts fondé sur la théorie*

des matrices aléatoires. PhD thesis, Université Paris Diderot, 2013.

[5] T. M. Holden, R. A. Holt, and A. P. Clarke, "Intergranular strains in Inconel-600 and the impact on interpreting stress fields in bent steam-generator tubing," *Mat. Sci. Eng. A*, vol. 246, no. 1, pp. 180–198, 1998.

[6] A. P. Arguelles and J. A. Turner, "Ultrasonic attenuation of polycrystalline materials with a distribution of grain sizes," *J. Acoust. Soc. Am.*, vol. 141, no. 6, pp. 4347–4353, 2017.

[7] R. Hill, "The elastic behaviour of a crystalline aggregate," *Proc. Phys. Soc. A*, vol. 65, no. 5, pp. 349–354, 1952.

[8] C. M. Kube and J. A. Turner, "Ultrasonic attenuation in polycrystals using a self-consistent approach," *Wave Motion*, vol. 57, pp. 182–193, 2015.

[9] K. F. Graff, "Waves in semi-infinite media," in *Wave motion in elastic solids*, ch. 6, pp. 311–393, Dover Publications Inc., 1975.

[10] D. Royer and D. Clorennec, "An improved approximation for the Rayleigh wave equation," *Ultrasonics*, vol. 46, no. 1, pp. 23–24, 2007.